



MINING ROCK PROPERTIES. ROCK MECHANICS AND GEOPHYSICS

Research paper

<https://doi.org/10.17073/2500-0632-2022-06-10>

UDC 550.834.08

**Amplitude-frequency response
of a helically-wound fiber distributed acoustic sensor (DAS)**

A. V. Chugaev , M. V. Tarantin

Mining Institute of the Ural Branch of the Russian Academy of Sciences, Perm, Russian Federation chugaev@mi-perm.ru**Abstract**

The goals of this study were to analyze the capabilities of DAS (distributed acoustic sensors) in resolving mining problems, compare them with existing seismoacoustic data collection systems, and prepare the basis for conducting seismoacoustic studies with recording by a fiber optic distributed system. This paper considers the capabilities of recording seismoacoustic responses using fiber optic distributed acoustic systems (DAS). Based on physical and geometrical analysis, the amplitude-frequency responses (characteristics) of recorded longitudinal waves for straight and helically-wound fibers were obtained. In the case of helically-wound fiber, the frequency response depends on several key factors: integrating the measured value along the fiber based on the measurement; the angle of incidence on the cable; and the winding angle of the fiber in the cable. An increase in the winding angle increases the uniformity of the amplitude-frequency characteristics of longitudinal waves both in terms of frequencies and angles of incidence. At the same time, helical winding changes the effective response spacing (gauge length). This makes it possible, by summing the responses of the straight and helically-wound fibers due to the overlap of the spectra, to record frequencies that are suppressed in case of separate recording. Based on the study results, a cable design was proposed to record broadband seismoacoustic responses enabling a wide range of mining and engineering problems to be resolved, and for seismic surveys both in wells and on the surface to be carried out.

Keywords

distributed acoustic sensor, fiber optic sensor, seismic exploration, borehole seismoacoustics, Rayleigh scattering, receiver directivity pattern

Acknowledgments

The reported study was funded by the Russian Foundation for Basic Research and the Perm Territory, Project Number 20-45-596032.

For citation

Chugaev A. V., Tarantin M. V. Amplitude-frequency response of a helically-wound fiber distributed acoustic sensor (DAS). *Mining Science and Technology (Russia)*. 2023;8(1):13–21. <https://doi.org/10.17073/2500-0632-2022-06-10>

СВОЙСТВА ГОРНЫХ ПОРОД. ГЕОМЕХАНИКА И ГЕОФИЗИКА

Научная статья

**Амплитудно-частотный отклик распределенного акустического сенсора DAS
со спиральной намоткой волокна**

А. В. Чугаев , М. В. Тарантин

Горный институт УрО РАН, г. Пермь, Российская Федерация chugaev@mi-perm.ru**Аннотация**

При проведении настоящего исследования была поставлена цель проанализировать возможности распределенных датчиков DAS при решении горнотехнических задач, сравнить с существующими сейсмоакустическими системами сбора данных и подготовить основу для проведения сейсмоакустических исследований с регистрацией оптоволоконной распределенной системой. Рассмотрены возможности регистрации сейсмоакустических сигналов с помощью оптоволоконных распределенных акустических систем. На основании физико-геометрического анализа получены амплитудно-частотные характеристики регистрируемых продольных волн для прямого и спирального волокна. Для спирального волокна амплитудно-частотные характеристики зависят от нескольких ключевых факторов: интегрирования измеряемого значения вдоль волокна на базе измерения, угла падения волны на кабель и угла намотки волокна в кабеле. Увеличение угла намотки повышает равномерность амплитудно-частотной характеристики



продольных волн как по частотам, так и по углам падения. В то же время спиральная намотка меняет эффективную базу измерения сигнала, что позволяет путем суммирования сигналов прямого и спирального волокна за счет перекрытия спектров выполнять регистрацию частот, подавляемых при раздельной записи. По результатам исследования предложена конструкция кабеля для регистрации широкополосных сейсмоакустических сигналов, с помощью которых можно решать обширный круг горнотехнических и инженерных задач, выполняя сейсморазведочные исследования как в скважинах, так и на поверхности.

Ключевые слова

распределенный акустический датчик, оптоволоконный сенсор, сейсморазведка, скважинная сейсмоакустика, рассеяние Рэлея, диаграмма направленности приемника

Благодарности

Исследование выполнено при финансовой поддержке РФФИ и Пермского края в рамках научного проекта №20-45-596032.

Для цитирования

Chugaev A. V., Tarantin M. V. Amplitude-frequency response of a helically-wound fiber distributed acoustic sensor (DAS). *Mining Science and Technology (Russia)*. 2023;8(1):13–21. <https://doi.org/10.17073/2500-0632-2022-06-10>

Introduction

Distributed systems for recording acoustic responses using optical fiber (DAS – distributed acoustic sensing) have been well known for several years [1–3]. However, their reduction to the practice of geophysical research requires certain practical problems related to the physical and geometric features of such systems to be resolved.

The recording of an acoustic response in a DAS system is carried out by analyzing the spectrum of Rayleigh light scattering in an optical fiber. This occurs when a light pulse of a given wavelength and duration passes. Longitudinal deformation of the fiber leads to a change in the amplitude and phase components of the frequency spectra of the reflection optical response [2]. Optical interferometry enables the magnitude of the strain in a certain section to be calculated. The position can be measured from the time of arrival of the backscattered optical pulse at a known velocity of light in the waveguide [4, 5]. The important characteristic of the system is Gauge Length L , which determined by specification of the interrogator. As a result, the stress distribution profile in the fiber at a certain point in time is calculated. The re-interrogation is limited by the time of arrival of the reflection response from the most remote section of the fiber optic cable. The velocity of light propagation in an optical fiber is 2×10^8 m/s. For a 1 km line, the double travel time of a light pulse is 10^{-5} s, and for 100 km it is 10^{-3} s. This is currently the limitation of the recorded response sampling by time.

The goals of this study were to analyze the capabilities of DAS in resolving mining problems, compare them with existing seismoacoustic data collection systems, and prepare the basis for conducting acoustic studies with recording by a fiber optic distributed system.

The frequency content of the responses recorded by fiber-optic sensors with linear fiber is considered

in [6–8]. Since DAS measurements involve averaging the measured parameter based on gauge length L , distortion of the acoustic response spectrum occurs at frequencies above 150–300 Hz [7, 9, 10]. Responses with a frequency not exceeding these values are suitable for resolving problems of oil seismic exploration [3, 11, 12] and monitoring ore deposits [13, 14]. In borehole and seismic exploration of mines, the upper limit of the frequency range of the useful response is 1000 Hz and higher [15–17]. Therefore, the possibility of using distributed fiber optic systems for solving mining problems needs to be considered and compared with existing seismoacoustic data collection systems. In addition, at the present time, the available literature provides no analysis of the amplitude-frequency characteristics of a helically-wound optic cable.

Acoustic pattern of straight fiber

DAS systems measure the deformation of an optical fiber along its axis. Thus, for longitudinal waves, the acoustic pattern is defined as $D_p(\alpha) = A_0 \cos^2 \alpha$, for transverse waves, $D_s(\alpha) = A_0 |\sin 2\alpha|$ [1, 18], where α is the angle between the fiber and the wave propagation vector; and A_0 is the amplitude of the incident wave. The incidence of a seismic wave on a linear section of an optical fiber is considered in [3, 11, 19]. Such a pattern significantly limits the range of possible seismic survey problems to be solved. Particularly, in many standard cases of seismic surveys, the target waves arrive along the normal line to the receiver line.

The use of special cables with non-standard fiber laying can expand the capabilities of fiber-optic systems for solving seismoacoustic problems. The cable design options are given in a patent [20]. For manufacturing, the most accessible way of laying a fiber in a cable is helical winding; field measurements are described in [21, 22].

Influence of winding angle on effective gauge length

With helical winding, the length of the fiber laid in a cable will be greater than the length of the cable. Thus, the effective value L_H (effective gauge length) of the rock mass associated with the cable will also change.

The decrease in the gauge length is proportional to the cosine of the winding angle:

$$L_H = L \cos \theta, \quad (1)$$

where θ is the angle of deviation of the fiber guide from the cable axis (for straight fiber $\theta = 0^\circ$)¹; L is gauge length along the fiber; L_H is gauge length along the cable with helically-wound fiber.

Influence of winding angle on cable sensitivity

When changing the cable directivity pattern due to winding, a single segment of the helix can be represented as a linear section with an equivalent distribution of sensitivity along the axes (Fig. 1). In a parametric form, the response energy will be distributed as follows:

$$E_z = E \cos^2 \theta; \quad (2)$$

$$E_r = E \sin^2 \theta; \quad (3)$$

$$E_{x,y} = \frac{1}{2} E \sin^2 \theta, \quad (4)$$

where E is full sensitivity; E_z , E_r , E_x , E_y are the sensitivities along z axis, in the plane perpendicular to z axis, along x and y axes, respectively.

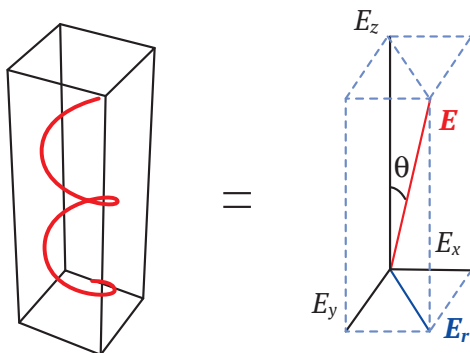


Fig. 1. Sensitivity distribution along the axes at helically-wound fiber

Per unit cable length, an increase in the recorded energy will occur due to an increase in the length of the fiber and the number of channels due to a decrease in the effective gauge length according to formula (1).

¹ In literature, there are two different ways of calculating the winding angle. Kuvshinov, Braid, Innanen et al. take 90° for a straight fiber, while in the study of Egorov, Tertysnikov, and others, 0° corresponds to a straight fiber. We stick to the latter version of the notation.

The algorithm for numerical calculation of the cable directivity pattern due to winding is given in [23, 24].

With an increase in the fiber winding angle, the sensitivity of the system along the normal to the cable axis appears. The directivity pattern for longitudinal waves changes from the pattern of a single-axis sensor towards the pattern of a pressure sensor having a uniform (spherical) pattern.

The sensitivity is evenly distributed between the axes at the value of the winding angle

$$\theta = \arccos\left(\frac{1}{\sqrt{3}}\right) \approx 54.7^\circ \quad [19, 23].$$

Thus, with a uniform directivity pattern (spherical) along one axis, the recorded energy will be 3 times less, and the response amplitude will decrease by $\sqrt{3}$ times.

The total response from the impact of a seismic wave with a helically-wound fiber consists of its interaction with equivalent sections decomposed along orthogonal axes. In the case of longitudinal waves, the responses will be added, and for transverse waves, they will be subtracted (Fig. 2).

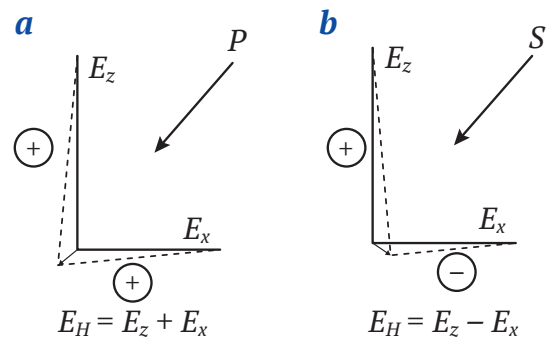


Fig. 2. Scheme of changing the length of the fiber under the influence of longitudinal (a) and transverse (b) waves

The directivity pattern is symmetrical with respect to the cable axis and depends on the angles of winding and seismic wave incidence in accordance with expressions (2–4):

$$D_P(\alpha, \theta) = \cos^2 \alpha \cos^2 \theta + \frac{1}{2} \sin^2 \alpha \cos^2 \theta; \quad (5)$$

$$D_S(\alpha, \theta) = \left| \sin 2\alpha \cos^2 \theta - \frac{1}{2} \sin 2\alpha \sin^2 \theta \right|, \quad (6)$$

where D_P, D_S are directivities for P and S waves, respectively; α is the angle between the cable and the seismic wave beam. Graphically, the patterns are shown in Fig. 3.

Note that the data obtained differs from that presented in study [23], where the polarity of S -wave response varies depending on the direction of propagation of the optical response in the fiber. However, this would mean that measurements on the same cable section when connecting from different ends of the optical line would give different results.

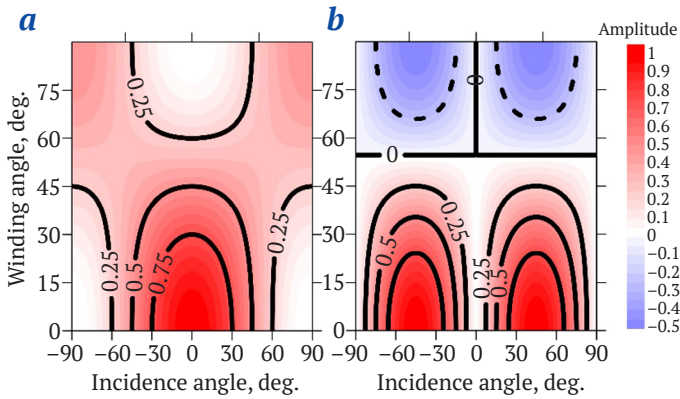


Fig. 3. Dependences of the sensitivity of a cable with helically-wound fiber on the angles of wave incidence and the fiber winding for *P* (a) and *S* (b) waves

Frequency characteristics of the recorded response for direct fiber

Let us consider the moment of time when a monochromatic elastic wave with oscillation frequency f has created longitudinal stresses in a fiber stretched along z axis. In this case, the amplitude of the recorded response will change according to the following expression:

$$A(x) = A_0 \sin(kz),$$

where $k = 2\pi f/V$ is wavenumber; A_0 is maximum response amplitude.

The amplitude of the response measured on a segment of length L is equal to the sum of the amplitudes along this segment:

$$A_L = A_0 \int_0^L \sin(kz) dz = A_0 \frac{V}{2\pi f} \left(1 - \cos\left(\frac{2\pi f L}{V}\right) \right). \quad (7)$$

Here we see that, firstly, as the frequency increases, the response amplitude decreases. Secondly, at points which satisfy the condition $L = n\lambda$, $n \in Z$, the function takes a null value. As a result, the amplitude-frequency characteristic (AFC) is complicated by the response attenuation sections as a result of the action of a rectangular window filter, which an extended linear receiver appears to be. The AFC for longitudinal waves propagating along the fiber at a velocity $V = 2500$ m/s and spacing $L = 10$ m is shown in Fig. 4.

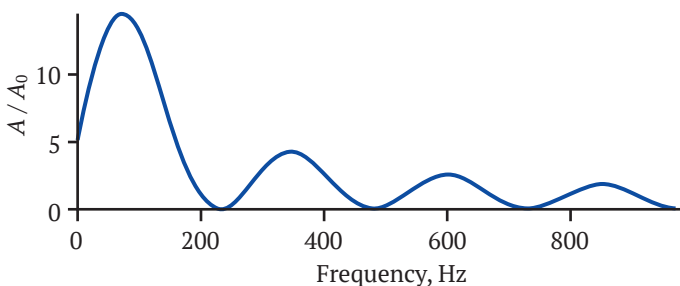


Fig. 4. Amplitude-frequency characteristic of a section of a straight fiber during the passage of a wave along it

The dependence of amplitude-frequency characteristics on the angle of incidence of a wave

When a linear receiver is located in the field of a harmonic wave (Fig. 5), the visible period will increase by increasing the angle α between the direction of wave propagation and the receiver line from 0° to 90° . The apparent frequency, in turn, will decrease:

$$f_a = f |\cos \alpha|. \quad (8)$$

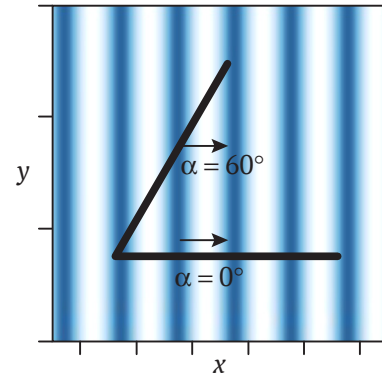


Fig. 5. Change in the visible period at different wave incidence angles

With regard to a section of a straight fiber and an arbitrary angle of incidence of wave α , the dependence of the AFC on the angle of incidence can be found as the product of the amplitude characteristic (7) and the directivity pattern, taking into account the apparent frequency instead of the actual one (8):

$$A_L(\alpha, f) = A_0 \frac{V}{2\pi f_a} \left(1 - \cos\left(\frac{2\pi L f_a}{V}\right) \right) D(\alpha). \quad (9)$$

The image of this dependence for longitudinal and transverse waves at $L = 10$ m, $V_p = 2500$ m/s, $V_s = 1500$ m/s is shown in Fig. 6. The image draws attention to the areas of rejection in the form of “smiles” and low sensitivity at angles close to 90° .

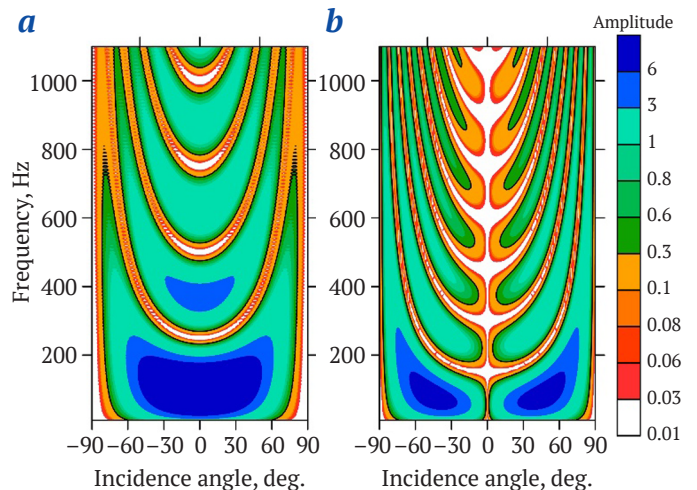


Fig. 6. Amplitude-frequency characteristic of a section of a straight fiber at different angles of incidence of an elastic wave for *P* (a) and *S* (b) waves

Amplitude-frequency response of helically-wound fiber

Next, let us consider a cable of radius r with helically-wound fiber, on which a wave is incident at an angle α . The angle of a wave incidence on separate small sections is equal to $\alpha + \varphi(z)$ (Fig. 7), where $\varphi(z)$ can be found through the derivative of the function describing the helically-wound fiber in plane view (z, x):

$$x(z) = r \sin\left(z \operatorname{tg} \frac{\theta}{r}\right), \quad (10)$$

from where

$$\varphi(z) = \operatorname{arctg}\left(\operatorname{tg} \theta \cos\left(z \operatorname{tg} \frac{\theta}{r}\right)\right). \quad (11)$$

The function $\varphi(z)$ takes values from $-\theta$ to θ , and provided that the wavelength is much larger than the pitch between the turns in the cable, the response will be equal to the sum

$$A_H(f, \theta, \alpha) = \sum_{\varphi=-\theta}^{\theta} A_L(f, \alpha + \varphi(z)) \Delta L(\varphi)/L, \quad (12)$$

where factor $\Delta L(\varphi)/L$ plays the role of a weighting factor depending on the proportion of the sections with a fixed angle φ in the total length of the fiber. The angle distribution can be found by calculating the derivative of function $z(x) = r \operatorname{ctg} \theta \operatorname{arcsin}(x/r)$:

$$\frac{dz}{dx} = \frac{\operatorname{ctg} \theta}{\sqrt{1 - \left(\frac{x}{r}\right)^2}}, \quad (13)$$

for which $x \in [-r, r]$ and the angles vary from $-\theta$ to θ . An example of φ distribution for a winding angle of 45° is shown in Fig. 8.

In the case of longitudinal waves, using formula (12), the amplitude-frequency characteristics were obtained for various winding angles of fiber in a cable (Fig. 9). With an increase in the winding angle, the rejection

bands are smoothed out. As a result, the response becomes more uniform in the angles of incidence. There are sensitivity curve dips in frequencies, although they are less pronounced than those for a straight fiber. This leaves room for spectrum whitening.

An important case here is the wave incidence angle of 90° , the response at which is shown separately in Fig. 10. It can be seen from the graphs that there are frequency bands, in which the response amplitude increases with increasing winding angle, and other bands where such amplification does not take place.

With an increase in the winding angle, the effective gauge length decreases in accordance with formula (1). This, in turn, leads to an increase in the frequency of the first minimum in the total frequency response. This fact makes it possible, when summing the responses from a straight and helically-wound fiber, to obtain a more uniform AFC (frequency response) in a wide range of the angles of wave incidence on the cable (Fig. 11). An exception relates to angles of incidence close to 90° , where the AFC depends only on helically-wound fiber.

Fiber bend radius in helically-wound cable

A standard telecommunication fiber has a certain range of standard sizes and labels. One of the main characteristics is the dependence of the response attenuation constant on the fiber bend radius.

The bend radius is determined in the plane where it is maximum. With uniform helical winding, the radius of bend is constant and coincides with the radius of the minimum curvature of the ellipse formed when the cable is intersected by a plane at the same angle as the winding angle (Fig. 12). Thus, the effective radius of curvature of a fiber will depend on the radius of the fiber in a cable r and the winding angle θ :

$$R_e = \frac{r}{\sin^2 \theta}. \quad (14)$$

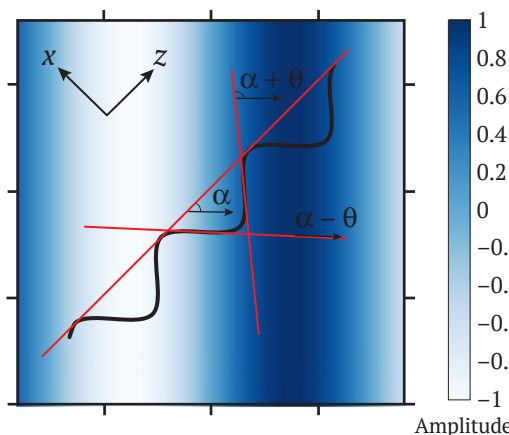


Fig. 7. Helically-wound fiber in the field of a plane elastic monochromatic wave

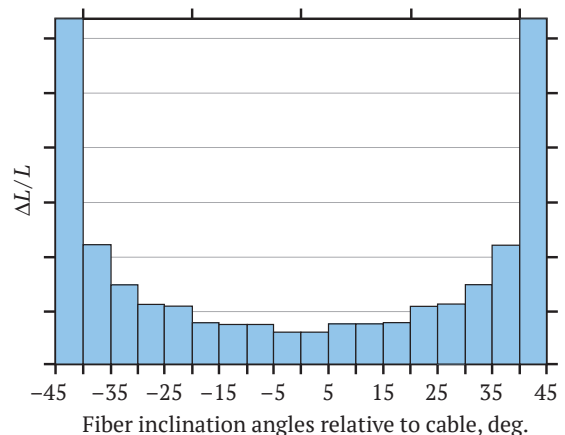


Fig. 8. Distribution of fiber inclination angles relative to cable axis at 45° helical winding

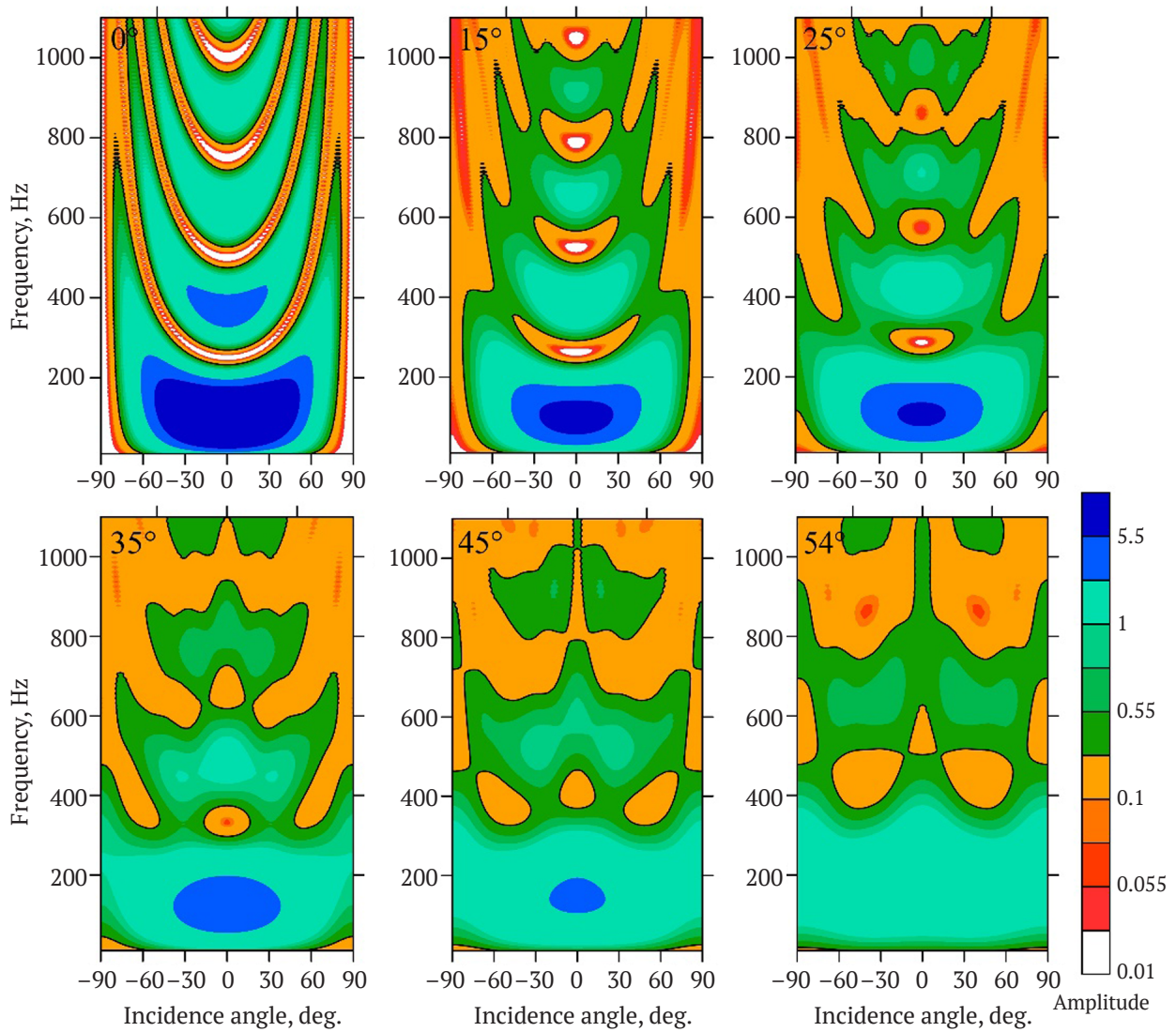


Fig. 9. Amplitude-frequency characteristics of a cable for different fiber winding angles

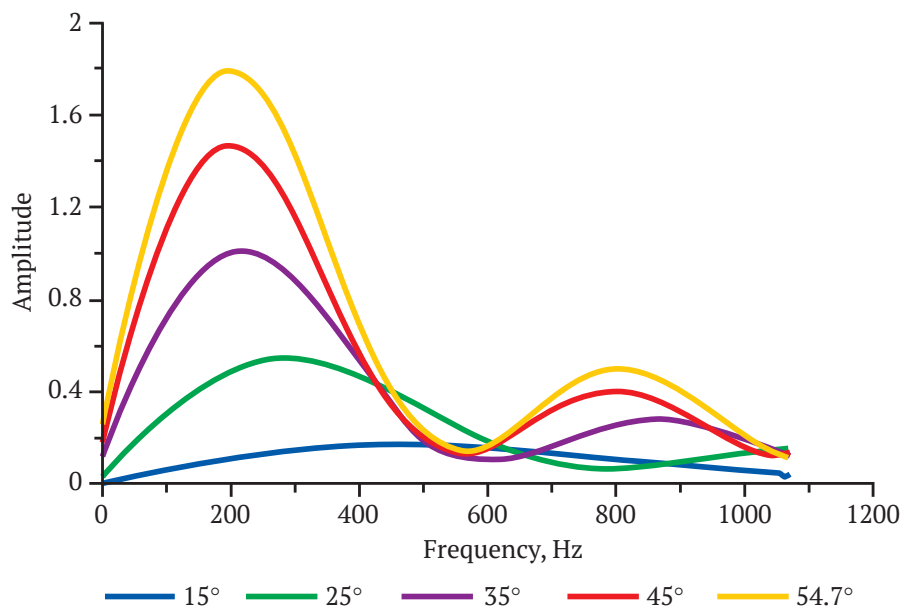


Fig. 10. Cross-sectional sensitivity of helically-wound fiber cable at various winding angles

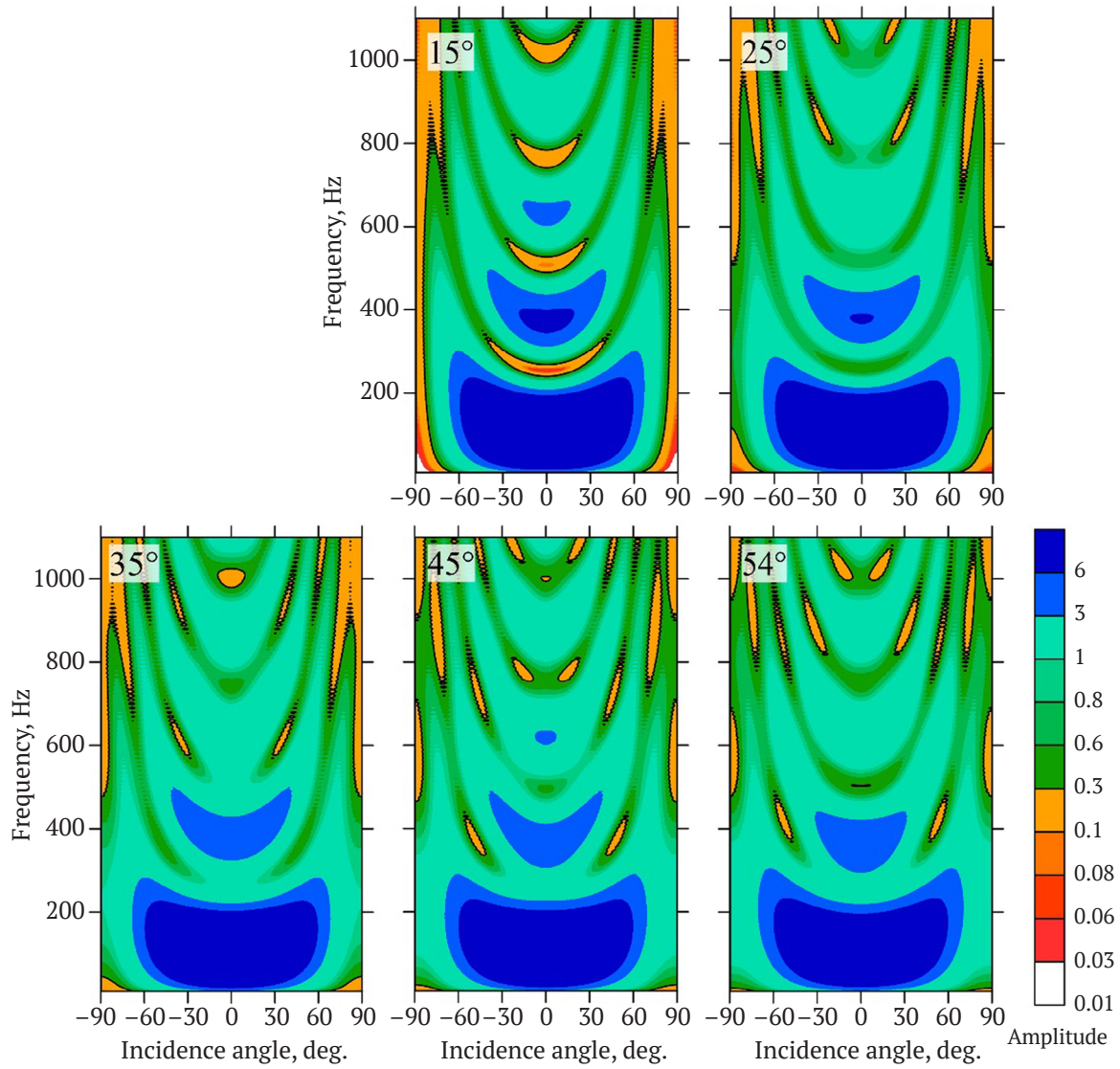


Fig. 11. Amplitude-frequency characteristics of the summed response from a straight and helically-wound fiber with different winding angles

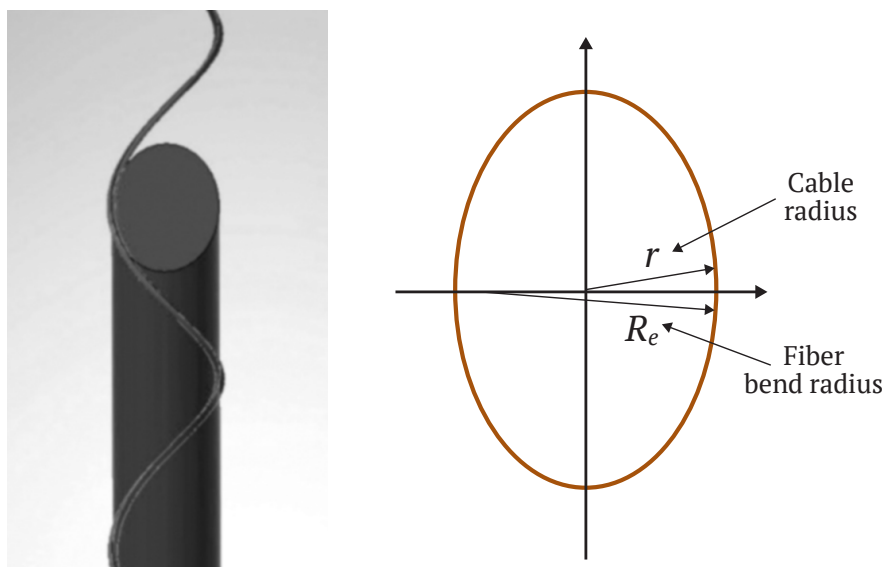


Fig. 12. Scheme for determining effective fiber bend radius



Taking R_c as a fixed value determined by the selected type of fiber, one can obtain the dependence of the cable radius on the winding angle θ : $r = R_c \sin^2 \theta$. The weight of such a cable will be proportional to $\sin^4 \theta$.

In the case of G657.A2 standard fiber, the bend radius at which there are no losses on a significant number of turns is 30 mm. Based on this value of the radius and the winding angle of 45° , a cable was designed containing both straight and helically-wound fibers. The outer diameter of the cable is 32.6 mm, and the weight is 721 kg/km. Such a cable can be used both for land seismic surveys and for downhole ones.

Conclusion

Analysis of the physical and geometric processes of recording acoustic responses by a distributed fiber optic system enabled the spatio-temporal characteristics of such systems to be obtained for straight and helically-wound fibers in a cable. The amplitude-frequency characteristics of the responses re-

corded by a helically-wound fiber depend on several key factors: integration of the measured value along the fiber on the gauge length; the angle of incidence of the wave on the cable; and the angle of winding of the fiber in the cable. It is possible to show that an increase in the winding angle increases the uniformity of the amplitude-frequency characteristic of longitudinal waves both in terms of frequencies and angles of incidence.

At the same time, helical winding changes the effective gauge length. By summing the responses of the straight and helically-wound fibers due to the overlap of the spectra, it is possible to record the frequencies suppressed in the case of separate recording.

Based on the results of the study, a cable design was proposed for recording broadband seismoacoustic responses, the use of which enables a wide range of mining and engineering problems to be resolved and for seismic surveys both in wells and on the surface to be carried out.

References

1. Mateeva A., Mestayer J., Cox B. et al. Advances in distributed acoustic sensing (DAS) for VSP. In: *SEG Technical Program Expanded Abstracts 2012*. Society of Exploration Geophysicists; 2012. <https://doi.org/10.1190/segam2012-0739.1>
2. Parker T., Shatalin S., Farhadiroushan M. Distributed Acoustic Sensing – a new tool for seismic applications. *First Break*. 2014;32(2):61–69. <https://doi.org/10.3997/1365-2397.2013034>
3. Wu X., Willis M.E., Palacios W. et al. Compressional- and shear-wave studies of distributed acoustic sensing acquired vertical seismic profile data. *The Leading Edge*. 2017;36(12):987–993. <https://doi.org/10.1190/tle36120987.1>
4. Hartog A., Kotov O.I., Liokumovich L.B. The optics of distributed vibration sensing. In: *Second EAGE Workshop on Permanent Reservoir Monitoring 2013 – Current and Future Trends*. Netherlands: EAGE Publications BV; 2013. <https://doi.org/10.3997/2214-4609.20131301>
5. Shatalin S.V., Treschikov V.N., Rogers A.J. Interferometric optical time-domain reflectometry for distributed optical-fiber sensing. *Applied Optics*. 1998;37(24):5600–5604. <https://doi.org/10.1364/AO.37.005600>
6. Dean T., Papp B., Hartog A. Wavenumber response of data recorded using distributed fibre-optic systems. In: *3rd EAGE Workshop on Borehole Geophysics*. Netherlands: EAGE Publications BV; 2015. <https://doi.org/10.3997/2214-4609.201412215>
7. Dean T., Cuny T., Hartog A. H. The effect of gauge length on axially incident P-waves measured using fibre optic distributed vibration sensing: Gauge length effect on incident P-waves. *Geophysical Prospecting*. 2017;65(1):184–193. <https://doi.org/10.1111/1365-2478.12419>
8. Bona A., Dean T., Correa J. et al. Amplitude and phase response of DAS receivers. In: *79th EAGE Conference and Exhibition 2017*. Netherlands: EAGE Publications BV; 2017. <https://doi.org/10.3997/2214-4609.201701200>
9. Stork A.L., Baird A.F., Horne S.A. et al. Application of machine learning to microseismic event detection in distributed acoustic sensing data. *Geophysics*. 2020;85(5):KS149–KS160. <https://doi.org/10.1190/geo2019-0774.1>
10. Näsholm S.P., Iranpour K., Wuestefeld A. et al. Array signal processing on distributed acoustic sensing data: Directivity effects in slowness space. *Journal of Geophysical Research: Solid Earth*. 2022;127(2). <https://doi.org/10.1029/2021JB023587>
11. Willis M.E., Barfoot D., Ellmauthaler A., Wu X. et al. Quantitative quality of distributed acoustic sensing vertical seismic profile data. *The Leading Edge*. 2016;35(7):605–609. <https://doi.org/10.1190/tle35070605.1>
12. Sudakova M.S., Belov M.V., Ponimaskin A.O. et al. Features of processing vertical seismic profiling data of offshore shallow wells with fiber-optic distributed systems. *Journal of Geophysics*. 2021;(6):110–118. (In Russ.)



13. Riedel M., Cosma C., Enescu N. et al. Underground Vertical Seismic Profiling with conventional and fiber-optic systems for exploration in the Kylylahti polymetallic mine, eastern Finland. *Minerals (Basel)*. 2018;8(11):538. <https://doi.org/10.3390/min8110538>

14. Bellefleur G., Schetselaar E., Wade D. et al. Vertical seismic profiling using distributed acoustic sensing with scatter-enhanced fibre-optic cable at the Cu–Au New Afton porphyry deposit, British Columbia, Canada. *Geophysical Prospecting*. 2020;68(1):313–333. <https://doi.org/10.1111/1365-2478.12828>

15. Yaroslavtsev A. G., Fatkin K. B. Mine seismic surveys for the control of safety pillars in potash mines. In: *Engineering and Mining Geophysics 2020*. European Association of Geoscientists & Engineers; 2020. <https://doi.org/10.3997/2214-4609.202051043>

16. Sanfirov I. A., Yaroslavtsev A. G., Chugaev A. V. et al. Frozen wall construction control in mine shafts using land and borehole seismology techniques. *Journal of Mining Science*. 2020;56(3):359–369. <https://doi.org/10.1134/S1062739120036641>

17. Chugaev A. V., Sanfirov I. A., Lisin V. P. et al. The integrated borehole seismic surveys at the verkhnekamskoye potassium salt deposit. In: *Lecture Notes in Networks and Systems*. Vol. 342. Cham: Springer International Publishing; 2022. Pp. 255–269. https://doi.org/10.1007/978-3-030-89477-1_25

18. Correa J., Egorov A., Tertyshnikov K. et al. Analysis of signal to noise and directivity characteristics of DAS VSP at near and far offsets – A CO2CRC Otway Project data example. *The Leading Edge*. 2017;36(12):962–1044. <https://doi.org/10.1190/tle36120994a1.1>

19. Kuvshinov B. N. Interaction of helically wound fibre-optic cables with plane seismic waves. *Geophysical Prospecting*. 2016;64(3):671–688. <https://doi.org/10.1111/1365-2478.12303>

20. den Boer J. J., Mateeva A., Pearce J. G. et al. *Detecting broadside acoustic signals with a fiber optical distributed acoustic sensing (DAS) assembly*. Standard Patent WO2013/090544/A1, 2013. URL: <https://patentimages.storage.googleapis.com/6a/52/dc/6513f050b2f66c/AU2012352253C1.pdf>

21. Tertyshnikov K., Bergery G., Freifeld B., Pevzner R. Seasonal effects on DAS using buried helically wound cables. In: *EAGE Workshop on Fiber Optic Sensing for Energy Applications in Asia Pacific*. European Association of Geoscientists & Engineers; 2020. <https://doi.org/10.3997/2214-4609.202070007>

22. Stork A. L., Chalari A., Durucan S. et al. Fibre-optic monitoring for high-temperature Carbon Capture, Utilization and Storage (CCUS) projects at geothermal energy sites. *First Break*. 2020;38(10):61–67. <https://doi.org/10.3997/1365-2397.fb2020075>

23. Baird A. Modelling the response of helically wound DAS cables to microseismic arrivals. In: *First EAGE Workshop on Fibre Optic Sensing*. European Association of Geoscientists & Engineers; 2020. <https://doi.org/10.3997/2214-4609.202030019>

24. Egorov A., Charara M., Alfataierge E., Bakulin A. Realistic modeling of surface seismic and VSP using DAS with straight and shaped fibers of variable gauge length. In: *First International Meeting for Applied Geoscience & Energy Expanded Abstracts*. Tulsa, OK, USA: Society of Exploration Geophysicists; 2021. Pp. 184–193. <https://doi.org/10.1190/segam2021-3576626.1>

Information about the authors

Alexander V. Chugaev – Cand. Sci. (Eng.), Head of the Sector of Shallow Well Research of the Department of Active Seismic Acoustics, Mining Institute of the Ural Branch of the Russian Academy of Sciences, Perm, Russian Federation; ORCID [0000-0002-7494-4042](https://orcid.org/0000-0002-7494-4042), Scopus ID [6602559950](https://scopus.org/6602559950); e-mail chugaev@mi-perm.ru

Mikhail V. Tarantin – Cand. Sci. (Eng.), Researcher, Department of Active Seismic Acoustics; Mining Institute of the Ural Branch of the Russian Academy of Sciences, Perm, Russian Federation; Scopus ID [36601605800](https://scopus.org/36601605800); e-mail muxaul20@rambler.ru

Received 04.06.2022

Revised 01.09.2022

Accepted 13.12.2022